Exosomes derived from stem cells from apical papilla promote craniofacial soft tissue regeneration through enhancing Cdc42-mediated vascularization

Yao Liu
Department of Paediatric Dentistry, School and Hospital of Stomatology, China Medical University; Liaoning Provincial Key Laboratory of Oral Diseases

Xueying Zhuang
Department of Paediatric Dentistry, School and Hospital of Stomatology, China Medical University; Liaoning Provincial Key Laboratory of Oral Diseases

Si Yu
Department of Paediatric Dentistry, School and Hospital of Stomatology, China Medical University

Ning Yang
Department of Paediatric Dentistry, School and Hospital of Stomotology, China Medical University

Jianhong Zeng
Department of Paediatric Dentistry, School and Hospital of Stomatology, China Medical University

Xu Chen (chenxu@cmu.edu.cn)
Department of Paediatric Dentistry, School of Stomotology, China Medical University
https://orcid.org/0000-0002-2158-8320

Research

Keywords: stem cells from apical papilla, exosome, vascularization, angiogenesis, tissue regeneration, cell migration, cell division cycle 42

Posted Date: November 18th, 2020

DOI: https://doi.org/10.21203/rs.3.rs-60880/v2

Version of Record: A version of this preprint was published on January 22nd, 2021. See the published version at https://doi.org/10.1186/s13287-021-02151-w.

Abstract

Background: Reconstruction of complex critical-size defects (CSD) in craniofacial region is a major challenge, and the soft tissue regeneration is crucial in determining the therapeutic outcome of craniofacial CSD. Stem cells from apical papilla (SCAP) are neural crest-derived mesenchymal stem cells (MSCs) which are homologous to craniofacial tissue, and represent a promising source for craniofacial tissue regeneration. Exosomes, which contained compound bioactive contents, are the key factors of stem cell paracrine action. However, the roles of exosomes derived from SCAP (SCAP-Exo) in tissue regeneration are not fully understood. Here, we explored the effects and underlying mechanisms of SCAP-Exo on CSD in maxillofacial soft tissue.

Methods: SCAP-Exo were isolated and identified by transmission electron microscopy and nanoparticle tracking analysis. The effects of SCAP-Exo on wound healing and vascularisation were detected by measuring wound area, histological and immunofluorescence analysis in the palate gingiva CSD of mice. Real-time live cell imaging and functional assays were used to assess the effects of SCAP-Exo on the biological functions of endothelial cells (ECs). Furthermore, the molecular mechanisms of SCAP-Exo mediated ECs angiogenesis in vitro was tested by immunofluorescence staining, Western blot and Pull-Down assays. Finally, in vivo experiments were carried out to verify whether SCAP-Exo could affect the vascularisation and wound healing through Cdc42.

Results: We showed that SCAP-Exo promoted tissue regeneration of palatal gingiva CSD by enhancing vascularisation in the early phase in vivo , and also indicated SCAP-Exo improved the angiogenic capacity of endothelial cells (ECs) in vitro . Mechanistically, SCAP-Exo elevated cell migration by improving cytoskeletal reorganization of ECs via cell division cycle 42 (Cdc42) signalling. Furthermore, we revealed that SCAP-Exo transferred Cdc42 into the cytoplasm of ECs, and the Cdc42 protein could be reused directly by the recipient ECs, which resulted in the activation of Cdc42 dependent filopodia formation and elevation of cell migration of ECs.

Conclusion: This study demonstrated that SCAP-Exo had a superior effect on angiogenesis and effectively promoted craniofacial soft tissue regeneration. These data provide a new option for SCAP-Exo to be used as a cell-free approach to optimize tissue regeneration in the clinic.

Background

Complex critical-size defects (CSD) in the craniofacial region caused by trauma, tumors, infection, and maxillofacial surgery seriously affect the physical appearance of patients and the function of the oral cavity, which pose major challenges to the reconstructive surgeon in the clinic [1-3]. The reconstruction of CSD in craniofacial region combined a variety of tissue regeneration, including bone, muscle, mucosa as well as skin. Although bone regeneration guided the structural stability and appearance of face, the overlying soft tissue is essential for bone regeneration, even restoration of orofacial function and aesthetic integrity [4]. Advances in tissue engineering have demonstrated that the successful regeneration

of soft tissues helps to prevent exogenous infection, provide sufficient nutrients, establish blood supply and so on [5]. Moreover, a large number of clinical studies have identified that the natural free flap technology effectively achieves soft tissue regeneration, which significantly improves the outcomes of craniofacial reconstruction [6]. It is well known that the vascular system is required for embryonic development and tissue regeneration, and adequate blood vessel formation could supply sufficient oxygen, nutrients, and eliminate metabolic waste [7]. Therefore, vascularization in the early phase of wound healing plays a critical role for the regeneration of craniofacial soft tissue [8]. The strategy based on bioactive factors derived from mesenchymal stem cells (MSCs) has been addressed as a promising approach for regenerative medicine [9]. Exosome, one of the most important extracellular microvesicles secreted from stem cells, contain lots of cytoplasmic contents including proteins, peptides, RNA, DNA and so on [10]. Increasing evidence demonstrates that exosomes have similar functions to donor MSCs, which regulate signal transcription and protein expression to mediate cellular functions of recipient cells [11]. In the process of tissue regeneration, exogenous MSCs are located around the endothelial cells (ECs), and promote angiogenesis by secreting exosome [12, 13]. In addition, compared to MSCs, exosomes may have a superior safety profile and can be steadily stored without losing cellular functions, which successfully overcome some of the major challengers related to cell based approach of regenerative medicine.

Stem cells from apical papilla (SCAP), as one type of neural crest-derived MSCs, are homologous to craniofacial region, which have been identified as a promising stem cell source for tissue engineering with high self-renewal and multi-lineage differentiation [14]. Since they are isolated from the highly vascularized developing apical tissue of immature permanent teeth, SCAP may have excellent properties for the promotion of angiogenesis [15]. Even in the stress microenvironment lacking oxygen, serum and glucose, SCAP also maintain biological activity and secrete a large amount of pro-angiogenesis growth factors, while the secretion of anti-angiogenesis growth factors is reduced to promote the ECs angiogenesis [16]. In addition, SCAP enhance vascularization to improve pulp-like tissue regeneration *in vivo*, emphasizing its promising role in tissue engineering [17]. It is well known that angiogenesis is a complex and highly precise process that includes endothelial progenitor cell activation, EC proliferation, migration, sprout, and neovascularization [18]. Among these, the migration of ECs mediated by cytoskeleton reorganization might play an important role in angiogenesis. The Rho GTPase family, including Cdc42, Rac1, and RhoA, are important molecular switches that regulate cytoskeletal reorganization [19]. Therefore, whether SCAP-Exo promotes angiogenesis and soft tissue regeneration, as well as its possible mechanisms are the main foci of this study.

In this study, we explored the role and potential application of SCAP-Exo for craniofacial soft tissue regeneration *in vivo.* Our findings suggested that SCAP-Exo improved cell migration of ECs and angiogenic capacity *via* cell division cycle 42 (Cdc42)-dependent cytoskeletal reorganization, which resulted in the promotion of tissue regeneration of palatal gingiva CSD. To the best of our knowledge, this is the first study in which SCAP-Exo can be used as a cell-free approach to optimize soft tissue regeneration in the clinic.

Materials And Methods

Animals

C57BL/6J mice and BALB/c nude mice were purchased from Vital River Laboratory Animals Technology (Beijing, China). All animal experiment protocols (2018029) were approved by the Institutional Animal Care and Use Committee of China Medical University.

Antibodies and reagents

Anti-CD9, CD63, Alix, calnexin, CD31, CD34, CD45, CD73, CD90 and CD105 antibodies were purchased from Abcam (Cambridge, UK). Anti-Ki-67, RhoA, Rac1, Cdc42 and β-actin antibodies were purchased from Cell Signaling Technology (Danvers, USA). Alexa Fluor 488 and Alexa Fluor 568 secondary antibodies were purchased from Proteintech (Rosemont, IL, USA). Goat anti-rabbit/anti-mouse IgG IRDyel 800cw secondary antibodies were purchased from Abbkine (Redlands, CA, USA). PKH-26 and PKH-67 kits were purchased from Sigma-Aldrich (St. Louis, MO, USA). Lipofectamine^{TM} RNAiMAX, FM^{TM}4-64FX and ActinGreen^{TM} 488 were purchased from Thermo Fisher (Eugene, Dregon, USA). SiCdc42, Cdc42-EGFP and Cdc42-mCherry fusion protein expression plasmids were purchased from GenePharma (Suzhou, China). Cdc42 inhibitor ML141 was purchased from MedChemExpress (Monmouth Junction, USA).

SCAP isolation and characterization

Human third molars with immature roots were obtained from healthy donors with an age range from 12 to 15 years in the clinic at the School of Stomatology affiliated with China Medical University. Informed consent was obtained from all patients and their parents. The apical papilla was gently separated and digested with dispase II (Boehringer Ingelheim, Mannheim, Germany) and collagenase type I (Worthington Biochemical Co., Lakewood, CO, USA). Single-cell suspensions were seeded and cultured in alpha-minimum essential medium (α-MEM, HyClone, Logan, UT, USA) supplemented with 15% (v/v) fetal bovine serum (FBS, MRC, Uruguay), 1% (v/v) penicillin-streptomycin solution (HyClone), 2 mM L-glutamine (Biosource/Invitrogen, USA), and 0.1 mM L-ascorbic acid (Sigma-Aldrich, St. Louis, MO, USA), and incubated at 37°C with 5% CO_2. The expression of MSC surface markers, including CD31, CD34, CD45, CD73, CD90, and CD105 was detected by flow cytometry. The multipotent differentiation potential of SCAP, including osteogenesis and adipogenesis, were evaluated using osteogenic and adipogenic differentiation media for four weeks. Alizarin red S and Oil red O staining were used to detect the formation of mineralized nodules and lipid droplets, respectively.

SCAP-Exo isolation and identification

SCAP were cultured in exosome-free medium for 48 h. The culture supernatant was collected and centrifuged at 4°C in three different speeds: 3,000 × *g* for 20 min, 20,000 × *g* for 30 min, and 120,000 × *g* for 2 h in an ultracentrifuge (Beckman Optima L-100XP, USA). Exosomes were resuspended in sterile PBS and stored at -80°C. SCAP-Exo were observed by transmission electron microscopy (TEM) (H-800, Hitachi,

Japan). A nanoparticle tracer analyzer (ZetaView, Germany) was used to measure the size of the particles. Exosomal surface markers, including CD9, CD63, and Alix were detected by western blotting. Cdc42 siRNA and Cdc42 inhibitor ML141 (20 μM) were used to treat SCAP (whole cells). The exosome-free medium was changed and the cells were cultured for 48 h. The culture supernatant was collected and centrifuged to isolate $SCAP^{siCdc42}$-Exo and $SCAP^{ML141}$-Exo.

Quantification of exosomes

Twenty microliters of SCAP-Exo were added to 50 μL protein lysate and lysed on ice for 1 h. BCA protein assay kit was used to generate the standard curve of protein concentration and was subsequently used to measure the concentration of SCAP-Exo.

SCAP-Exo treatment in wound healing of CSD in the palatal gingiva

The wound model was identical to a previous study [20]. Full-thickness circular gingival wounds (soft tissue defects) with a diameter of 2.0 mm were made in the palates of C57BL/6J mice using a biopsy punch (n = 5). SCAP-Exo or $SCAP^{siCdc42}$-Exo was suspended in PBS at a concentration of 1 μg/μL. Forty microliters SCAP-Exo, $SCAP^{siCdc42}$-Exo, or PBS (as control) were injected submucosally into four symmetrical sites around the wounds after they were created, according to previous protocol [21], so that 40 μg exosomes were applied locally on each wound. Mice were sacrificed 7 days post-operation, fixed in 4% paraformaldehyde, and decalcified with 10% ethylenediaminetetraacetic acid solution. The samples were embedded in paraffin, sectioned and stained with haematoxylin and eosin (H&E). In addition, the samples were embedded in optimal cutting temperature compound and sectioned. The frozen sections were stained with immunofluorescent CD31, an endothelial marker of micro-vessels, and the CD31 positive area was analysed using the Image J software (1.50i, National Institutes of Health, Bethesda, MD, USA).

In vivo tracking experiment

PKH-26-labelled SCAP-Exo or PBS (as control) was injected submucosally into four symmetrical sites around the wounds once after the wounds were created. Mice were sacrificed after 7 days post operation. Frozen sections and fluorescence images were used to observe the fate of SCAP-Exo.

Real-time live-cell imaging (RT-LCI)

Human umbilical vein endothelial cells (HUVECs) were seeded into a 35-mm dish (81158, Ibidi, Germany) and stained with FM™ 4-64FX. SCAP-Exo were labelled with PKH-67 and added to the HUVECs. The process of HUVECs taking up SCAP-Exo was observed under the laser confocal microscope (ECLIPSE Ti2, Nikon, Japan) for 30 min continuously.

Western blot analysis

The protein concentration was detected using a BCA protein assay kit. Proteins (20 μg) were loaded onto a 12% sodium dodecyl sulphate-polyacrylamide gel for electrophoresis, and then transferred to polyvinylidene difluoride membranes. The membranes were exposed to the appropriate primary and secondary antibodies. Finally, the bands were revealed using an Odyssey CLx instrument (LI-COR, Lincoln, NE, USA). The density of the bands was measured with Image J to quantify protein expression.

Tube formation assay

Matrigel (50 μL) (#356234, BD Biosciences, San Jose, CA) was precoated in each well of a 96-well plate and polymerized at 37 °C. HUVECs and SCAP-Exo-pretreated HUVECs were seeded at a density of 1.5×10^4 cells/well and cultured for 8 h. Photos of tube formation were taken by a stereoscopic microscope (ECLIPSE TE2000-S, Nikon, Japan). The indexes of tube formation were analysed using Image J.

Matrigel plug assay

Matrigel (200 μL) (#356231, BD Biosciences, San Jose, CA) was mixed with SCAP-Exo, $SCAP^{siCdc42}$-Exo, $SCAP^{ML141}$-Exo or PBS on ice. The mixtures were injected subcutaneously into the dorsum of BALB/c nude mice *(n* = 5). After 14 days, the matrigel plugs were extracted. H&E staining was used and the number of vessels in the matrigel was counted.

Cell proliferation assay

Cell proliferation was measured using the Cell Counting Kit-8 (CCK-8) and Ki-67 staining assay. HUVECs were seeded into 96-well plates at a density of 2,000 cells/well, and cultured with SCAP-Exo. The plates were incubated for 24, 48, and 72 h. CCK-8 solution (Dojindo, Kumamoto, Japan) was added and incubated in the dark. The absorbance of each well was measured at 450 nm using a microplate reader (Tecan, Salzburg, Austria). In addition, HUVECs (2×10^4/well) were seeded on glass coverslips placed inside a 12-well plate and cultured to the logarithmic phase. Thereafter, cells were fixed and stained with Ki-67 immunofluorescent antibody. The number of Ki-67-positive cells was indicated as a percentage of the total cell number.

Cell migration assay

Cell migration was measured using the transwell cell migration and scratch wound healing assay. HUVECs were seeded into the upper transwell insert of a 24-well plate at a density of 1×10^4 cells/well. SCAP-Exo were added into the lower chamber and incubated for 24 h. Thereafter, cells in the transwell chamber were removed. After staining with crystal violet, the number of cells migrating below the transwell layer was counted. Moreover, HUVECs (5×10^5/well) were seeded into a 6-well plate and a scratch in the cells was made with a 200 μL sterile tip. The serum-free medium containing SCAP-Exo was then replaced. After 0, 12, and 24 h, the boundaries of the scratches were recorded and the wound closure rates were measured and calculated using Image J.

Pull-Down assay

RhoA/Rac1/Cdc42 Activation Assay Combo Biochem Kit (Cytoskeleton, Denver, CO, USA) was used following the manufacturer's instructions. Briefly, the equivalent protein amounts of lysate were added to a pre-determined amount of rhotekin-RBD (for RhoA activation) or PAK-PBD beads (for Rac1 and Cdc42 activation) and incubated at 4 °C on a rotator for 1 h. Next, the beads were centrifuged and washed. The bead pellets were resuspended with 20 μL loading buffer and boiled. The samples were then analysed by western blot.

F-actin immunofluorescence staining

HUVECs were fixed for 30 min and stained with ActinGreen^{TM} 488 at 4 °C for 30 min. Pseudopodia formation was observed by fluorescence microscopy (ECLIPSE 80i, Nikon, Japan). We counted the number of filopodia and used Image J software to quantitatively analyze the length of filopodia.

Plasmid transfection and fluorescence co-localization

The Cdc42-EGFP or Cdc42-mCherry fusion protein expression plasmids were transfected into SCAP to extract SCAP$^{Cdc42\text{-}EGFP}$-Exo or SCAP$^{Cdc42\text{-}mCherry}$-Exo. SCAP$^{Cdc42\text{-}EGFP}$-Exo was added to HUVECs and passaged to the 6th passage. SCAP$^{Cdc42\text{-}mCherry}$-Exo was added to HUVECs overnight. Cells were incubated with Cdc42 primary antibody and fluorescent secondary antibody. The co-localization of Cdc42 and Cdc42-mCherry was observed by confocal microscopy (ECLIPSE Ti2, Nikon).

Statistical analysis

All data were recorded as the mean ± standard deviation (SD). Comparisons between two groups were analysed using an independent two-tailed Student's *t* test, and comparisons between more than two groups were analysed using one-way analysis of variance (ANOVA) with SPSS 20.0 (SPSS Inc., Chicago, IL, USA). A value of $P < 0.05$ was statistically significant.

Results

Characterization of SCAP and Identification of SCAP-Exo

The SCAP had spindle-shaped cells in primary culture (Fig. S1a). Under *in vitro* osteogenic and adipogenic induction, SCAP formed mineralized nodes and oil droplets, as assessed by Alizarin red S staining and oil red O staining (Fig. S1b-c). Flow cytometry analysis showed that SCAP expressed MSC surface markers, including CD73, CD90, and CD105, while the hematopoietic markers CD31, CD34, and CD45 were absent (Fig. S1d).

We isolated extracellular vesicles (EVs) from the culture supernatant of SCAP. The EVs exhibited a bilayer membrane and a cup-plate-shaped structure under TEM (Fig. S2a). Nanoparticle tracking analysis showed that EVs with diameters of about 120.1 nm accounted for 97.2% of nanoparticles, and the mean

diameter of EVs was 139.2 ± 62.5 nm (Fig. S2b). Western blot analysis showed that EVs expressed the exosomal markers Alix, CD9, and CD63, and failed to express calnexin (Fig. S2c). Therefore, following the guidelines from the minimal information from studies of EVs [22], we identified the EVs isolated from SCAP as exosomes.

SCAP-Exo promoted vascularization to accelerate tissue regeneration of palatal gingiva

We locally infused SCAP-Exo into CSD in the palatal gingiva of mice and analysed the therapeutic affects at 1, 3, and 7 days (Fig. 1a). The *in vivo* tracking experiment showed that PKH-26-labelled SCAP-Exo could exist in palatial gingiva defects until 7 days post operation (Fig. S3). We found that the wound area of the palatal gingiva was significantly reduced in the SCAP-Exo infusion group at 3 and 7 days post-wounding compared to that in the controls (Fig. 1b). The newly formed and integral epidermis and connective tissues were observed in the SCAP-Exo group using H&E staining at 7 days post-wounding, while the formation of epidermis and connective tissues were markedly delayed in the controls (Fig. 1b). We further focused on vascularization in the early phase of healing of the palatal gingiva CSD. H&E staining showed that there were significantly more newly formed blood vessels in the gingiva wounds in the SCAP-Exo group than in the controls at 1 and 3 days post-wounding (Fig. 1c). Immunostaining confirmed that the percentage of the CD31 positive area was significantly increased in the SCAP-Exo group at 1 and 3 days post-wounding (Fig. 1d). Therefore, our data indicated that SCAP-Exo promoted vascularization in the early phase of healing and accelerated tissue regeneration of the palatal gingiva.

SCAP-Exo improved the angiogenic capacity of HUVECs

To determine the effects of SCAP-Exo on angiogenesis, we used SCAP-Exo to treat HUVECs *in vitro.* RT-LCI showed that SCAP-Exo were endocytosed into the cytoplasm of HUVECs (Fig. S4a-e). Based on the analysis of the X-T, Y-T and X-Y-Z image axes, we observed the entire process of SCAP-Exo taken into HUVECs (Fig. S4f-h). To select an optimal concentration of SCAP-Exo, different doses (5-20 μg/mL) of SCAP-Exo were added to HUVECs. We found that SCAP-Exo increased the expression of the angiogenic protein CD31 in HUVECs in a dose-dependent manner (Fig. S5). Therefore, we used 20 μg/mL SCAP-Exo in subsequent experiments.

CD31, also named platelet endothelial cell adhesion molecule-1, is a crucial angiogenic marker expressed in vascular endothelial cells [23]. Western blot analysis showed that the expression levels of CD31 in HUVECs were markedly upregulated in the SCAP-Exo treated group, when compared to those in the non-treated controls (Fig. 2a). In order to detect the SCAP-Exo effects on the vascular lumen formation *in vitro*, we performed the matrigel tube formation assay and indicated that SCAP-Exo treatment significantly increased the indexes of vascular lumen forming compared to those of the controls, as shown by increased total tube length, total meshes, total branches, total nodes and total junctions (Fig. 2b). Furthermore, we examined the effects of SCAP-Exo on blood vessel formation *in vivo*. We found that in the SCAP-Exo group, there were markedly increased newly formed blood vessels in the subcutaneously implanted matrigel compared to that in the controls (Fig. 2c). H&E staining also showed significantly increased number of vascular lumen structure with more aggregated red blood cells in the SCAP-Exo-

treated group compared to those in the non-treated controls (Fig. 2d). These data suggested that SCAP-Exo improved the angiogenic capacity of ECs.

SCAP-Exo mediated cell migration contributing to HUVEC angiogenesis

It is well known that cell migration and cell proliferation play important roles in angiogenesis of ECs [24]. To clarify how SCAP-Exo improved the angiogenic capacity of HUVECs, we first tested the cell proliferation of HUVECs in both the SCAP-Exo and control groups. We found that there was no significant change in the proliferation rate of HUVECs in the SCAP-Exo group when compared to that in the controls, as assessed by CCK-8 assay and Ki-67 staining (Fig. 3a, b). However, the transwell cell migration assay showed that the number of migrated cells in the SCAP-Exo-treated HUVECs was higher than that in the non-treated HUVECs (Fig. 3c). The wound healing rate of HUVECs in the SCAP-Exo group was also significantly increased at 12 and 24 h, compared to that in the controls (Fig. 3d). These experimental data indicated that SCAP-Exo upregulated cell migration of ECs to promote angiogenesis.

SCAP-Exo improved cell migration of HUVECs *via* Cdc42-mediated cytoskeletal reorganization

The reorganization of the actin cytoskeleton and pseudopodia formation provides a driving force for cell migration [25]. Accordingly, F-actin immunofluorescence staining showed that the actin cytoskeleton and newly formed filopodium were increased in the cytoplasm of HUVECs treated with SCAP-Exo when compared to those in untreated HUVECs, as indicated by the upregulation of the number of filopodia per cell and filopodia length (Fig. 4a). The Rho GTPase family acts as a molecular switch to regulate cytoskeletal reorganization, contributing to cell migration, including RhoA, Rac1 and Cdc42 [26]. Therefore, we tested the expression of Rho GTPases in both the SCAP-Exo-treated HUVECs and the controls. Interestingly, the Pull-Down assay and western blot showed that the expression levels of total Cdc42 and Cdc42-GTP were elevated in SCAP-Exo-treated HUVECs when compared to those in the non-treated HUVECs, while there was no significant difference in the expression levels of RhoA and Rac1 (Fig. 4b). To determine the role of Cdc42 in SCAP-Exo-mediated EC migration, we used Cdc42 siRNA and a Cdc42 inhibitor (ML141) to downregulate Cdc42 expression in SCAP-Exo. We showed that Cdc42 siRNA and Cdc42 inhibitor (ML141) downregulated the Cdc42 expression in SCAP-Exo (Fig. 4c). The total Cdc42 and Cdc42-GTP expression levels of HUVECs were not changed with the treatment of $SCAP^{siCdc42}$-Exo or $SCAP^{ML141}$-Exo, when compared with those in non-treated HUVECs (Fig. 4d). Moreover, we found that $SCAP^{siCdc42}$-Exo or $SCAP^{ML141}$-Exo induced significantly decreased number and length of filopodia of HUVECs compared with the $SCAP^{vehicle}$-Exo-treated HUVECs (Fig. 4e). Moreover, the scratch wound healing assay showed that the knockdown of Cdc42 in SCAP-Exo blocked the $SCAP^{vehicle}$-Exo-mediated elevation of cell migration in HUVECs (Fig. 4f). The *in vitro* Matrigel tube formation assay indicated that $SCAP^{siCdc42}$-Exo- and $SCAP^{ML141}$-Exo-treated HUVECs had a reduced capacity in forming vascular lumens compared to the $SCAP^{vehicle}$-Exo group, as shown by decreased total tube length, total meshes, total branches, total nodes, and total junctions (Fig. 4g). Furthermore, H&E staining showed a significantly decreased formation of vascular lumen structure in the $SCAP^{siCdc42}$-Exo and $SCAP^{ML141}$-Exo groups

compared to that in the $SCAP^{vehicle}$-Exo group *via* the Matrigel plug assay (Fig. 4h). These data indicated that SCAP-Exo improved cytoskeletal reorganization and contributed to cell migration of ECs *via* Cdc42 signalling.

To explore the detailed mechanism of SCAP-Exo-induced Cdc42 expression in HUVECs, we used western blot analysis to examine the protein levels of Cdc42 in SCAP and SCAP-Exo. We found that Cdc42 was steadily expressed in SCAP and SCAP-Exo derived from different SCAP populations, and Cdc42 had higher expression level in SCAP-Exo than that in SCAP (Fig. 4i). Furthermore, we transfected SCAP with a Cdc42 enhanced green fluorescent protein (Cdc42-EGFP) plasmid and isolated $SCAP^{Cdc42\text{-}EGFP}$-Exo. We used $SCAP^{Cdc42\text{-}EGFP}$-Exo to treat HUVECs and found that the Cdc42-EGFP protein derived from SCAP-Exo was transferred to HUVECs and expressed continuously in the cytoplasm of passage 0 (P0), P3 and P6 HUVECs (Fig. 4j). In addition, we produced $SCAP^{Cdc42\text{-}mCherry}$-Exo by transfecting SCAP with a Cdc42-mCherry fluorescent protein plasmid and then used $SCAP^{Cdc42\text{-}mCherry}$-Exo to treat HUVECs. Laser confocal microscope showed the co-localization of Cdc42-mCherry (red) and Cdc42 (green) in the cytoplasm of SCAP-Exo-treated HUVECs (Fig. 4k). Taken together, these experimental data indicated that SCAP-Exo elevated cell migration by the transfer of Cdc42 protein to improve the cytoskeletal reorganization of ECs.

SCAP-Exo facilitated tissue regeneration of palatal gingiva *via* Cdc42-mediated vascularization

We wondered whether the Cdc42 derived from SCAP-Exo contributed to the accelerated tissue regeneration of the palatal gingiva, so we produced Cdc42 knockdown SCAP-Exo ($SCAP^{siCdc42}$-Exo) and infused $SCAP^{siCdc42}$-Exo or SCAP-Exo locally into the gingival wounds (Fig. 5a). We found that gingival healing was significantly delayed in the $SCAP^{siCdc42}$-Exo group at 3 and 7 days post-wounding compared to the SCAP-Exo group (Fig. 5b). H&E staining showed that in the $SCAP^{siCdc42}$-Exo group, newly formed epidermis and a thin layer of connective tissue was observed at 7 days post-wounding, while in the SCAP-Exo group, the epidermis tissue was intact and continuous, and the connective tissues were markedly thickened (Fig. 5b). We further verified vascularization in the early phase of wound healing in both the $SCAP^{siCdc42}$-Exo and SCAP-Exo groups. H&E staining showed that the $SCAP^{siCdc42}$-Exo group exhibited less newly formed blood vessels than in the SCAP-Exo group at 1 and 3 days post-wounding (Fig. 5c). Immunostaining confirmed that knockdown of Cdc42 in SCAP-Exo blocked the SCAP-Exo-mediated upregulation of vascularization in the early phase, as indicated by the decreased percentage of CD31 positive area in the $SCAP^{siCdc42}$-Exo group at 1 and 3 days post-wounding compared to that in the SCAP-Exo group (Fig. 5d). Therefore, our data indicated that SCAP-Exo facilitated tissue regeneration of palatal gingiva *via* Cdc42-mediated vascularization.

Discussion

Angiogenesis is the formation and remodelling of new blood vessels and capillaries from the growth of existing blood vessels, which plays a crucial role in wound healing [27]. In the process of wound healing,

rapid and sufficient vascularization not only provides oxygen and nutrients to the surviving cells, but also eliminates necrotic substances and controls infections [28]. Thus, the stimulation of vascularization in the early phase is the most important factor for the therapeutic effects of MSC-based tissue engineering. SCAP are the postnatal population of epidermal neural crest stem cells, which have a high capability to promote angiogenesis when compared with bone marrow mesenchymal stem cells (BMMSCs) [29]. Meanwhile, the neural crest-derived MSCs carry neurovascular factors such as vascular endothelial growth factor, platelet derived growth factor, and brain-derived neurotrophic factor, which mediate the angiogenic process to improve tissue regeneration and treat ischemic diseases [30-32]. Exosomes have similar cellular properties to the parent cell [33]. Here, we showed that the local infusion of SCAP-Exo promoted new blood vessel formation at 1 and 3 days post-wounding, and accelerated the healing of CSD in the palatal gingiva. Therefore, as the important paracrine factor secreted from SCAP, SCAP-Exo have an excellent effect on promoting angiogenesis. Moreover, we pursued a cell-free approach, finding inspiration from the consensus that SCAP-Exo have the advantages of low immune rejection, high stability, ease of accessing the wound surface and absence of vascular obstruction [34-37]. Since the strength of wound margins is crucial for evaluating wound healing in palatal gingiva, further study is needed to evaluate the tissue healing and functional recovery of the palate CSD to fully demonstrate the effects of SCAP-Exo on soft tissue regeneration, including the strength of wound margins, the structure of collagen fibrils, and so on.

In the process of blood vessel formation, the proliferation and cell migration of ECs interact with angiogenic factors and result in the formation of new capillaries. Thereafter, capillaries are covered by smooth muscle cells to form mature blood vessels with viscoelasticity and contractility [24]. Here, we showed originally that SCAP-Exo specially increased the cell migration of ECs, contributing to ECs angiogenesis, while there were no marked effects on the cell proliferation of ECs. Cytoskeletal reorganization and pseudopodia formation play critical roles in cell migration [25]. Additionally, the formation of filopodia in SCAP-Exo-treated ECs was elevated when compared to that in non-treated ECs, which confirmed the promotive effects of SCAP-Exo on cell migration. Several extracellular signals are involved in modulating the activity of microfilament-binding proteins to re-organize the cytoskeleton. The family of Rho GTPases, as the key downstream target, is currently believed to promote cytoskeletal organization [26]. Cdc42, Rac1 and RhoA are the main members of the Rho GTPase family, which play different roles in cytoskeletal reorganization [38]. Therefore, we examined the expression levels of the family of Rho GTPases and found that only Cdc42 signalling were significantly upregulated in SCAP-Exo-treated ECs compared to those in the controls. The activation of Cdc42 leads to the combination of WASP and Arp2/3 complex by binding to the GTPase binding domain of WASP, and directly regulates the polymerization of globular actin, resulting in the formation of fibrous Actin (F-actin), Which causes the cytoplasmic membrane to protrude outwards and form filopodia [39, 40]. Filopodia formation is the initial step of cell movement, and is helpful in determining the direction of cell migration [41]. Moreover, Cdc42 was also involved in the multi-mechanisms of angiogenesis. Cdc42 deletion increased ADAM17-mediated VEGFR2 shedding, and reduced VEGFR2 expression on the EC surface, which indicated that Cdc42 was essential for VEGFR2-mediated signal transduction in blood vessel formation [42]. Here, we

revealed a potential mechanism by which infusion of SCAP-Exo promoted the migration of ECs by activating Cdc42, leading to accelerated healing of CSD in the palatal gingiva by enhancing vascularization.

Exosomes, served as systemic cell-cell communication mediators, play an important role in MSC transplantation [43]. The underlying mechanisms are complicated, but may include releasing the contents to the recipient cell by endocytosis or direct combination with the molecule receptor of the recipient cell [21, 44-45]. Here, we showed that SCAP-Exo were internalized into the cytoplasm of HUVECs. We further used the co-localization and continued passage experiment to indicate that Cdc42 derived from SCAP-Exo was directly transferred into HUVECs and reused by HUVECs. Additionally, it is worth mentioning that increased amount of Cdc 42 protein was enriched in SCAP-Exo when compared with SCAP, which suggested SCAP-Exo might have a superior promotion on angiogenesis. Cdc42, a kind of Rho GTPase, continuously switches between the active GTP-binding state and the inactive GDP-binding state; the GTP situation can allow downstream signalling activation [46]. Interestingly, we found that not only the total Cdc42, but the Cdc42-GTP expression levels were also significantly increased in SCAP-Exo-treated ECs. In addition to the total Cdc42-mediated GDP-GTP switch, guanine nucleotide exchange factors (GEFs), guanine nucleotide activating proteins (GAPs) and guanine dissociation inhibitors (GDIs) may contribute to active GTP-binding state of ECs [47]. The detailed mechanism of the induction of the active GTP binding state requires further investigation.

In this study, we found for the first time that Cdc42 protein was expressed in MSC-derived exosomes, and further revealed that exosomal Cdc42 could be transferred into ECs and reused by recipient ECs, which contributed to the cell migration of ECs to promote angiogenesis. Being distinct from the intercellular Cdc42 protein, Cdc42 in donor MSC-derived exosomes could mediate the cellular functions of recipient cells. These results indicated that MSC-derived exosomes could play a crucial role in biological crosstalk between recipient cells, which enriched the theoretical basis of MSC-derived bioactive factor based tissue regeneration. At the same time, we showed that SCAP-Exo enhanced the cell migration-mediated angiogenesis of ECs, which resulted in the promotion effects on gingiva tissue regeneration of palatal CSD. In addition, gingival fibroblasts, which maintain the structural integrity of mucosa tissue, play crucial roles in the gingiva regenerative process. Therefore, we could not rule out the regulatory effects of SCAP-Exo treatment on fibroblast functions.

With the development of regenerative medicine, stem cell-based strategy has changed to a strategy based on bioactive factors. MSC-derived exosomes, containing many bioactive factors, could be a potential experimental strategy for soft tissue regeneration in the future. However, more studies will be needed before the clinical application of SCAP-Exo on angiogenesis and soft tissue regeneration.

Conclusion

In summary, this study showed that local infusion of SCAP-Exo accelerated tissue regeneration of the palatal gingiva CSD by promoting vascularization in the early phase. Mechanistically, SCAP-Exo

improved cell migration through enhancing cytoskeletal reorganization of ECs by directly transferring Cdc42 into the cytoplasm of recipient ECs. These data suggested SCAP-Exo could present a superior promotion on angiogenesis and provide a new strategy for using SCAP-Exo as a cell-free approach to optimize tissue regeneration in the clinic.

Abbreviations

CSD: critical-size defects; MSCs: mesenchymal stem cells; ECs: endothelial cells; SCAP: stem cells from apical papilla; SCAP-Exo: exosomes derived from stem cells from apical papilla; Cdc42: cell division cycle 42; TEM: transmission electron microscopy; H&E: haematoxylin and eosin; RT-LCI: real-time live-cell imaging; HUVECs: human umbilical vein endothelial cells; CCK-8: cell counting kit-8; SD: standard deviation; ANOVA: one-way analysis of variance; EGFP: enhanced green fluorescent protein; BMMSCs: bone marrow mesenchymal stem cells; F-actin: fibrous actin; GEFs: guanine nucleotide exchange factors; GAPs: guanine nucleotide activating proteins; GDIs: guanine dissociation inhibitors.

Declarations

Ethics approval and consent to participate This research was conducted according to the Institutional Animal Care and Use Committee of China Medical University (2018029).

Consent for publication Not applicable.

Competing interests The authors declare that they have no competing interests.

Acknowledgements: The authors thank Dr Weidong Zhao, Department of Developmental Cell Biology, School of Life Sciences, China Medical University for his insights and revision.

Authors' contributions: YL: Conception and design, data collection, data analysis and interpretation, manuscript writing, final approval of manuscript. XYZ: Data collection, data analysis and interpretation, manuscript writing, final approval of manuscript. SY: Data collection, provision of study material. NY: Data collection, provision of study material. JHZ: Data collection, provision of study material. XC: Conception and design, financial support, data analysis and interpretation, final approval of manuscript. All authors read and approved the final manuscript.

Funding: This work was supported by grants from the National Natural Science Foundation of China (82071100 to X.C.), and the Department of Science and Technology of Liaoning Province (2018225061 to X.C.).

Availability of data and materials The data used to support the findings of this study are available from the corresponding author upon reasonable request.

References

1. Wolff J, Farre-Guasch E, Sandor GK, Gibbs S, Jager DJ, Forouzanfar T. Soft tissue augmentation techniques and materials used in the oral cavity: An overview. *Implant Dent.* 2016; 25: 427-34.
2. Barnes LA, Marshall CD, Leavitt T, Hu MS, Moore AL, Gonzalez JG, Longaker MT, Gurtner GC. Mechanical forces in cutaneous wound healing: Emerging therapies to minimize scar formation. *Adv Wound Care.* 2018; 7: 47-56.
3. Schmitz JP, Hollinger JO. The critical size defect as an experimental model for craniomandibulofacial nonunions. *Clin Orthop Relat Res*. 1986: 299-308.
4. Shestak KC. Soft-tissue reconstruction of craniofacial defects. *Clin Plast Surg.* 1994; 21: 107-11.
5. Brouwer KM, Lundvig DM, Middelkoop E, Wagener FA, Von den Hoff JW. Mechanical cues in orofacial tissue engineering and regenerative medicine. *Wound Repair Regen.* 2015; 23: 302-11.
6. Seim NB, Old M, Petrisor D, Thomas W, Naik A, Mowery AJ, Kang S, Li R, Wax MK. Head and neck free flap survival when requiring interposition vein grafting: A multi-instiutional review. *Oral Oncol*. 2020; 101: 104482.
7. Carmeliet P, Jain RK. Molecular mechanisms and clinical applications of angiogenesis. *Nature*. 2011; 473:298-307.
8. Kasper FK, Melville J, Shum J, Wong M, Young S. Tissue engineered prevascularized bone and soft tissue flaps. *Oral Maxillofac Surg Clin North Am*. 2017; 29: 63-73.
9. 9. L PK, Kandoi S, Misra R, S V, K R, Verma RS. The mesenchymal stem cell secretome: A new paradigm towards cell-free therapeutic mode in regenerative medicine. *Cytokine Growth Factor Rev*. 2019; 46: 1-9.
10. Sluijter JP, Verhage V, Deddens JC, van den Akker F, Doevendans PA. Microvesicles and exosomes for intracardiac communication. *Cardiovasc Res*. 2014; 102: 302-11.
11. Chew JRJ, Chuah SJ, Teo KYW, Zhang S, Lai RC, Fu JH, Lim LP, Lim SK, Toh WS. Mesenchymal stem cell exosomes enhance periodontal ligament cell functions and promote periodontal regeneration. *Acta Biomater*. 2019; 89: 252-64.
12. Merckx G, Hosseinkhani B, Kuypers S, Deville S, Irobi J, Nelissen I, Michiels L, Lambrichts I, Bronckaers A. Angiogenic effects of human dental pulp and bone marrow-derived mesenchymal stromal cells and their extracellular vesicles. *Cells*. 2020; 9: 312.
13. 13. Ryu B, Sekine H, Homma J, Kobayashi T, Kobayashi E, Kawamata T, Shimizu T. Allogeneic adipose-derived mesenchymal stem cell sheet that produces neurological improvement with angiogenesis and neurogenesis in a rat stroke model. *J Neurosurg*. 2019; 132(2): 442-55.
14. 14. Sonoyama W, Liu Y, Fang D, Yamaza T, Seo BM, Zhang C, Liu H, Gronthos S, Wang CY, Wang S, Shi S. Mesenchymal stem cell-mediated functional tooth regeneration in swine. *PloS One*. 2006; 1: e79.
15. Sonoyama W, Liu Y, Yamaza T, Tuan RS, Wang S, Shi S, Huang GT. Characterization of the apical papilla and its residing stem cells from human immature permanent teeth: A pilot study. *J Endod.* 2008; 34: 166-71.

16. Bakopoulou A, Kritis A, Andreadis D, Papachristou E, Leyhausen G, Koidis P, Geurtsen W, Tsiftsoglou A. Angiogenic potential and secretome of human apical papilla mesenchymal stem cells in various stress microenvironments. *Stem Cells Dev*. 2015; 24: 2496-512.
17. Hilkens P, Bronckaers A, Ratajczak J, Gervois P, Wolfs E, Lambrichts I. The angiogenic potential of DPSCs and SCAPs in an in vivo model of dental pulp regeneration. *Stem Cells Int*. 2017; 2017: 2582080.
18. Xue C, Shen Y, Li X, Li B, Zhao S, Gu J, Chen Y, Ma B, Wei J, Han Q, Zhao RC. Exosomes derived from hypoxia-treated human adipose mesenchymal stem cells enhance angiogenesis through the PKA signaling pathway. *Stem Cells Dev*, 2018; 27: 456-465.
19. Abraham S, Scarcia M, Bagshaw RD, McMahon K, Grant G, Harvey T, Yeo M, Esteves FOG, Thygesen HH, Jones PF, Speirs V, Hanby AM, Selby PJ, Lorger M, Dear TN, Pawson T, Marshall CJ, Mavria G. A Rac/Cdc42 exchange factor complex promotes formation of lateral filopodia and blood vessel lumen morphogenesis. *Nat Commun*. 2015; 6: 7286.
20. Li CH, Amar S. Role of secreted frizzled-related protein 1 (sfrp1) in wound healing. *J Dent Res*. 2006; 85: 374-8.
21. Kou X, Xu X, Chen C, Sanmillan ML, Cai T, Zhou Y, Giraudo C, Le A, Shi S. The Fas/Fap-1/Cav-1 complex regulates IL-1RA secretion in mesenchymal stem cells to accelerate wound healing. *Sci Transl Med.* 2018; 10: eaai8524.
22. Théry C, Witwer KW, Aikawa E, Alcaraz MJ, Anderson JD, Andriantsitohaina R, et al. Minimal information for studies of extracellular vesicles 2018 (MISEV2018): A position statement of the international society for extracellular vesicles and update of the MISEV2014 guidelines. *J Extracell Vesicles*. 2018; 7: 1535750.
23. Kim SJ, Kim JS, Papadopoulos J, Wook Kim S, Maya M, Zhang F, He J, Fan D, Langley R, Fidler IJ. Circulating monocytes expressing CD31: implications for acute and chronic angiogenesis. *Am J Pathol*. 2009; 174: 1972-80.
24. Carmeliet P. Mechanisms of angiogenesis and arteriogenesis. *Nat Med*. 2000; 6: 389-395.
25. Ridley AJ, Schwartz MA, Burridge K, Firtel RA, Ginsberg MH, Borisy G, Parsons JT, Horwitz AR. Cell migration: Integrating signals from front to back. *Science*. 2003; 302: 1704-9.
26. Nobes CD, Hall A. Rho, rac and cdc42 GTPases: Regulators of actin structures, cell adhesion and motility. *Biochem Soc Trans*. 1995; 23: 456-9.
27. Velazquez OC. Angiogenesis and vasculogenesis: Inducing the growth of new blood vessels and wound healing by stimulation of bone marrow-derived progenitor cell mobilization and homing. *J Vasc Surg*. 2007; 45(Suppl A): A39-47.
28. Zimta AA, Baru O, Badea M, Buduru SD, Berindan-Neagoe I. The role of angiogenesis and pro-angiogenic exosomes in regenerative dentistry. *Int J Mol Sci*. 2019; 20: 406.
29. Janebodin K, Zeng Y, Buranaphatthana W, Ieronimakis N, Reyes M. VEGFR2-dependent angiogenic capacity of pericyte-like dental pulp stem cells. *J Dent Res*. 2013; 92: 524-31.

30. Gandia C, Armiñan A, García-Verdugo JM, Lledó E, Ruiz A, Miñana MD, Sanchez-Torrijos J, Payá R, Mirabet V, Carbonell-Uberos F, Llop M, Montero JA, Sepúlveda P. Human dental pulp stem cells improve left ventricular function, induce angiogenesis, and reduce infarct size in rats with acute myocardial infarction. *Stem Cells*. 2008; 26: 638-45.
31. Shi H, Li X, Yang J, Zhao Y, Xue C, Wang Y, He Q, Shen M, Zhang Q, Yang Y, Ding F. Bone marrow-derived neural crest precursors improve nerve defect repair partially through secreted trophic factors. *Stem Cell Res Ther*. 2019; 10: 397.
32. Sui B, Chen C, Kou X, Li B, Xuan K, Shi S, Jin Y. Pulp stem cell-mediated functional pulp regeneration. *J Dent Res*. 2019; 98: 27-35.
33. Yu B, Zhang X, Li X. Exosomes derived from mesenchymal stem cells. *Int Mol Sci.* 2014; 15: 4142-57.
34. Burger D, Viñas JL, Akbari S, Dehak H, Knoll W, Gutsol A, Carter A, Touyz RM, Allan DS, Burns KD. Human endothelial colony-forming cells protect against acute kidney injury: Role of exosomes. *Am J Pathol.* 2015; 185: 2309-23.
35. De Jong OG, Van Balkom BW, Schiffelers RM, Bouten CV, Verhaar MC. Extracellular vesicles: Potential roles in regenerative medicine. *Front Immunol*. 2014; 5: 608.
36. Rani S, Ritter T. The exosome - a naturally secreted nanoparticle and its application to wound healing. *Adv Mater*. 2016; 28: 5542-52.
37. Xin H, Li Y, Chopp M. Exosomes/miRNAs as mediating cell-based therapy of stroke. *Front Cell Neurosci*. 2014; 8: 377.
38. Aspenstrom P, Fransson A, Saras J. Rho GTPases have diverse effects on the organization of the actin filament system. *Biochem J*. 2004; 377(Pt 2): 327-37.
39. Kroon J, Schaefer A, van Rijssel J, Hoogenboezem M, van Alphen F, Hordijk P, Stroes ESG, Strömblad S, van Rheenen J, van Buul JD. Inflammation-sensitive myosin-x functionally supports leukocyte extravasation by cdc42-mediated icam-1-rich endothelial filopodia formation. *J Immunol.* 2018; 200: 1790-801.
40. Rohatgi R, Ma L, Miki H, Lopez M, Kirchhausen T, Takenawa T, Kirschner MW. The interaction between N-WASP and the ARP2/3 complex links Cdc42-dependent signals to actin assembly. *Cell*. 1999; 97: 221-31.
41. Yamaguchi H, Condeelis J. Regulation of the actin cytoskeleton in cancer cell migration and invasion. *Biochim Biophys Acta*. 2007; 1773: 642-52.
42. Jin Y, Liu Y, Lin Q, Li J, Druso JE, Antonyak MA, Meininger CJ, Zhang SL, Dostal DE, Guan JL, Cerione RA, Peng X. Deletion of Cdc42 enhances ADAM17-mediated vascular endothelial growth factor receptor 2 shedding and impairs vascular endothelial cell survival and vasculogenesis. *Mol Cell Biol*. 2013; 33: 4181-97.
43. Liu S, Liu D, Chen C, Hamamura K, Moshaverinia A, Yang R, Liu Y, Jin Y, Shi S. MSC transplantation improves osteopenia via epigenetic regulation of Notch signaling in lupus. *Cell Metab*. 2015; 22: 606-18.

44. Chen CY, Rao SS, Ren L, Hu XK, Tan YJ, Hu Y, Luo J, Liu YW, Yin H, Huang J, Cao J, Wang ZX, Liu ZZ, Liu HM, Tang SY, Xu R, Xie H. Exosomal DMBT1 from human urine-derived stem cells facilitates diabetic wound repair by promoting angiogenesis. *Theranostics*. 2018; 8: 1607-23.
45. Skog J, Würdinger T, van Rijn S, Meijer DH, Gainche L, Sena-Esteves M, Curry WT Jr, Carter BS, Krichevsky AM, Breakefield XO. Glioblastoma microvesicles transport RNA and proteins that promote tumour growth and provide diagnostic biomarkers. *Nat Cell Biol*. 2008; 10: 1470-6.
46. Boissier P, Huynh-Do U. The guanine nucleotide exchange factor Tiam1: A janus-faced molecule in cellular signaling. *Cell Signal*. 2014; 26: 483-91.
47. Bishop AL, Hall A. Rho GTPases and their effector proteins. *Biochem J*. 2000; 348(Pt 2): 241-55.

Supplementary Information

Additional file 1: Figure S1. Characterization of SCAP. The SCAP had spindle-shaped cells in primary culture. Under *in vitro* osteogenic and adipogenic induction, SCAP formed mineralized nodes and oil droplets, as assessed by Alizarin red S staining and oil red O staining. Flow cytometry analysis showed that SCAP expressed MSC surface markers, including CD73, CD90, and CD105, while the hematopoietic markers CD31, CD34, and CD45 were absent.

Additional file 2: Figure S2. Identification of SCAP-Exo. The Morphology of SCAP-Exo was observed under transmission electron microscopy. The size and concentration of SCAP-Exo were measured by nanoparticle tracking analysis. Western blot showed that the exosomal surface markers Alix, CD9, CD63 were expressed in SCAP-Exo, while calnexin was negatively expressed.

Additional file 3: Figure S3. The fate of SCAP-Exo *in vivo*. The *in vivo* tracking experiment showed that PKH-26-labeled SCAP-Exo were observed in palatial gingiva defects at 7 day post-wounding.

Additional file 4: Figure S4. SCAP-Exo were endocytosed by HUVECs. Real-time live-cell imaging under laser confocal microscope showed that an increasing number of SCAP-Exo were endocytosed by HUVECs. The analysis of X-T axis and Y-T axis showed the process in which SCAP-Exo was taken up by HUVECs. The three-dimensional scanning showed SCAP-Exo existing in the cytoplasm of HUVECs.

Additional file 5: Figure S5. SCAP-Exo improved the expression level of the angiogeneic protein CD31 in HUVECs. Western blot showed that SCAP-Exo upregulated the expression levels of CD31 in HUVECs in a dose-dependent manner.

Additional file 6: Figure S6. Schematic diagram of SCAP-Exo promoted the vascularization of regenerative tissue by triggering cell migration of vascular endothelial cells. SCAP-Exo was endocytosed by ECs, and transferred Cdc42 protein into recipient ECs to activate Cdc42/WASP/ARP2/3 cascade-mediated cytoskeletal reorganization and fliopodia formation, which resulted in elevation of the cell migration of ECs and promotion of the vascularization of regenerative tissue.

Figures

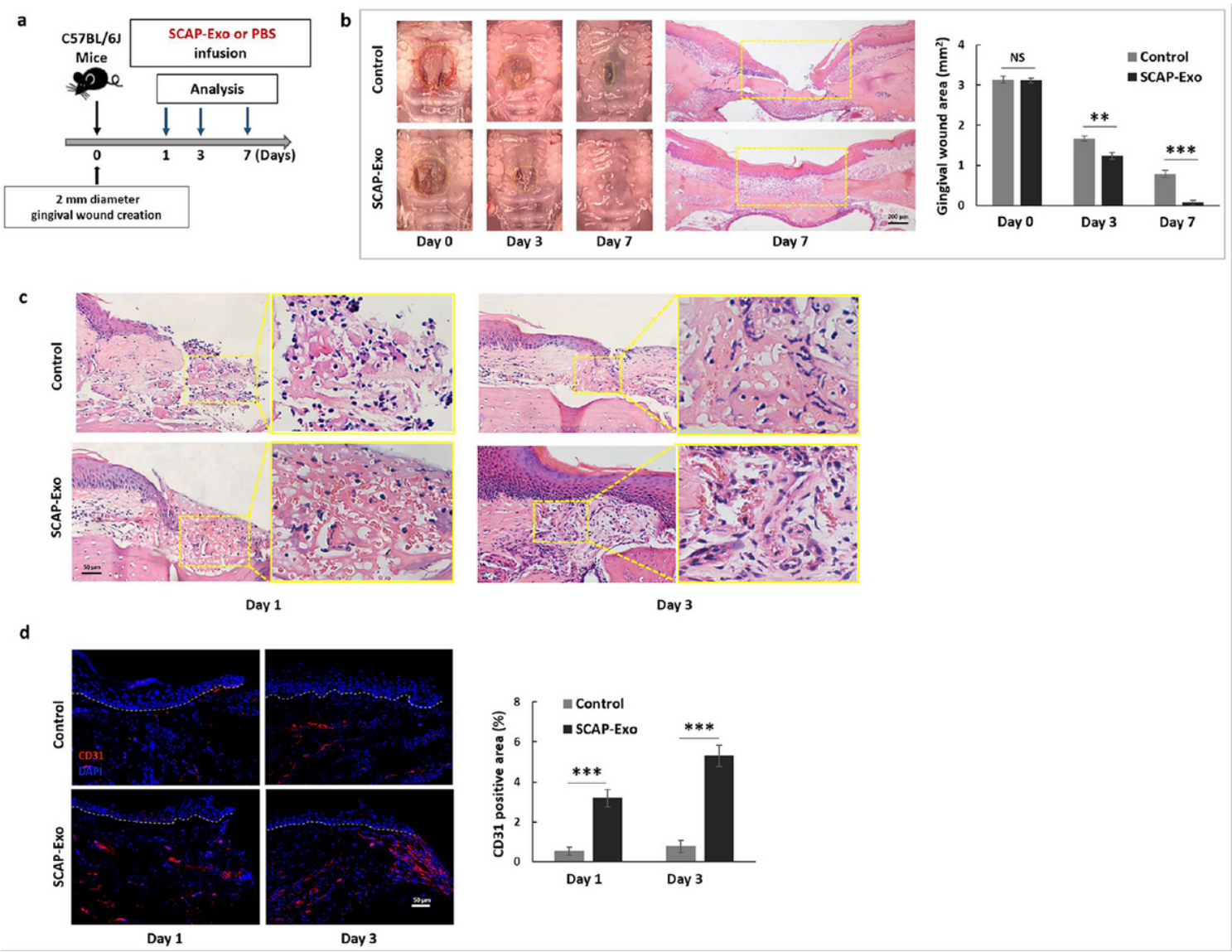

Figure 1

SCAP-Exo promoted angiogenesis to accelerate wound healing in palatal gingiva. a Schema indicating the experimental design for SCAP-Exo infusion in the gingival wound in palate of mice. b Representative images and quantification of gingival wound area in the control and SCAP-Exo groups. The wound healing of palatal gingiva was significantly accelerated in the SCAP-Exo group at 3, 7 days post-wounding compared to the control group. Scale bar = 200 μm. c The histological views showed lots of newly formed blood vessels containing red blood cells in the gingival wound of SCAP-Exo group at 1, 3 days post-wounding when compared with control group. Scale bar = 50 μm. d Immunofluorescence staining and quantification showed that the percentage of CD31 positive area (red) in the SCAP-Exo group was higher than that in the control group at 1, 3 days post-wounding. The epidermis and connective tissues were separated by the white dotted line in the images. Slides were counterstained with

DAPI (blue). Scale bar = 50 μm. n = 5 in each group. NS: P > 0.05, **P < 0.01, ***P < 0.001; Error bars: mean ± SD.

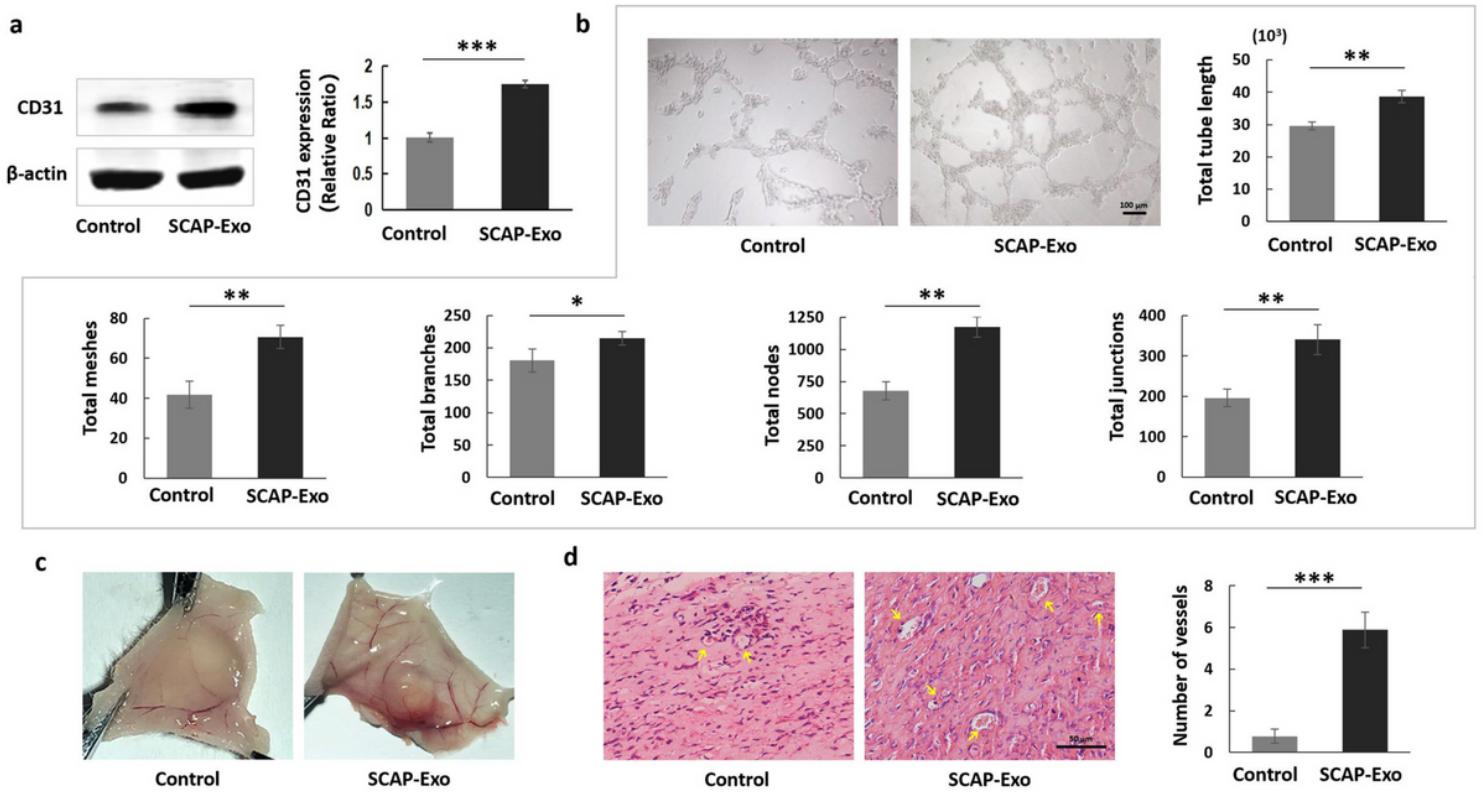

Figure 2

SCAP-Exo improved the angiogenic capacity of HUVECs. a Western blot analysis showed that SCAP-Exo treatment upregulated the expression levels of CD31 in HUVECs. b The in vitro tube formation assay showed that the untreated HUVECs were scattered and formed less lumens, while SCAP-Exo-treated HUVECs formed complete lumens. The data including total tube length, total meshes, total branches, total nodes and total junctions were increased in SCAP-Exo-treated HUVECs when compared with untreated HUVECs. Scale bar = 100 μm. c Representative images of matrigel plugs showed that there were more newly formed blood vessels in the SCAP-Exo group when compared with the control group. d H&E staining showed that there were more vascular lumens (yellow arrow) containing red blood cells in the SCAP-Exo group compared to the control group. Scale bar = 50 μm. n = 5 in each group. *P < 0.05, **P < 0.01, ***P < 0.001, Error bars: mean ± SD.

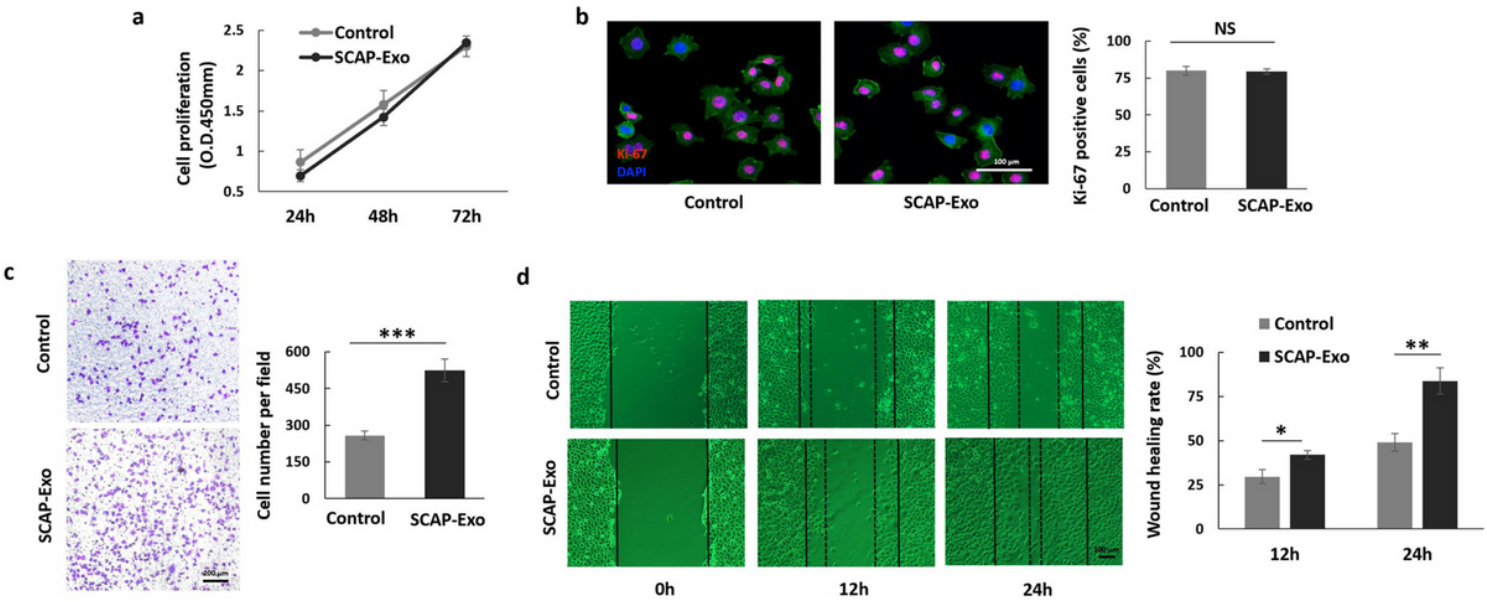

Figure 3

SCAP-Exo mediated cell migration contributing to HUVECs angiogenesis. a CCK-8 assay showed that SCAP-Exo treatment had no effect on the proliferation rate of HUVECs when compared with control group. b Ki-67 staining assay showed the percentage of Ki-67 positive cells (red) in the SCAP-Exo group was not different from that in the control group. Slides were counterstained with DAPI (blue) and F-actin (green). Scale bar = 100 μm. c Transwell cell migration assay showed that SCAP-Exo treatment upregulated the cell motility of HUVECs compared to control group. Scale bar = 200 μm. d Representative images of scratch wound healing assay showed that the wound healing rate in the SCAP-Exo group was increased at 12 h and 24 h when compared with the control group. Scale bar = 100 μm. n = 5 in each group. NS: $P > 0.05$, *$P < 0.05$, **$P < 0.01$, ***$P < 0.001$; Error bars: mean ± SD.

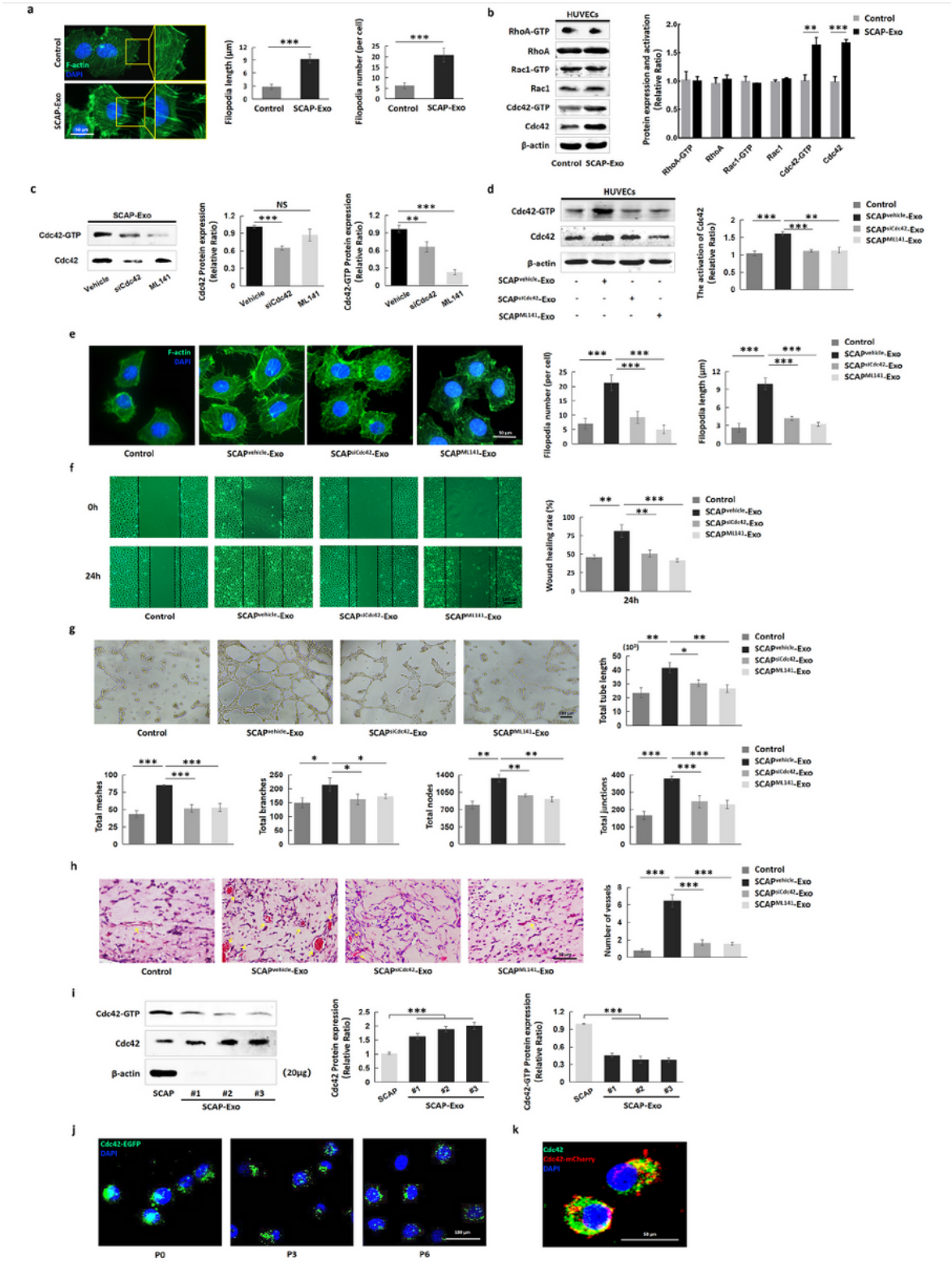

Figure 4

SCAP-Exo improved cell migration of HUVECs via Cdc42-mediated cytoskeletal reorganization. a F-actin immunofluorescence staining showed that the actin cytoskeleton and filopodia formation (green) was obviously increased in the SCAP-Exo-treated HUVECs compared to the control HUVECs. The number of filopodia for per cell and the filopodia length of SCAP-Exo-treated HUVECs was higher than that of control HUVECs. Scale bar = 50 μm. b Western blot and Pull-down assay showed that the expression levels of

Cdc42-GTP and Cdc42 were elevated in the SCAP-Exo-treated HUVECs, while the expression of RhoA and Rac1 had no significant changes. c Western blot and Pull-down assay showed that siCdc42 significantly reduced the Cdc42 and Cdc42-GTP expression in SCAP-Exo, while ML141 mainly declined the expression level of Cdc42-GTP in SCAP-Exo. d The expression levels of Cdc42 and Cdc42-GTP were significantly upregulated in the SCAPvehicle-Exo-treated HUVECs compared to the control HUVECs, while the SCAPsiCdc42-Exo and SCAPML141-Exo did not increase the expression levels of Cdc42 and Cdc42-GTP in HUVECs. e F-actin immunofluorescence staining showed that the actin cytoskeleton and the number and length of filopodia of HUVECs were increased in the SCAPvehicle-Exo group compared to the control group, while the SCAPsiCdc42-Exo- or SCAPML141-Exo-treated HUVECs were decreased compared to the SCAPvehicle-Exo group. Scale bar = 50 μm. f Representative images of scratch wound healing assay showed that the HUVEC migration in the SCAPvehicle-Exo group was higher than that in the control group, while the migration ability of HUVECs in the SCAPsiCdc42-Exo or SCAPML141-Exo group were reduced when compared with the SCAPvehicle-Exo group at 24 h. Scale bar = 100 μm. g The in vitro tube formation assay showed that SCAPsiCdc42-Exo- and SCAPML141-Exo-treated HUVECs had a reduced capacity of forming vascular lumen compared to the SCAPvehicle-Exo group. Scale bar = 100 μm. h H&E staining showed that there were less vascular lumens (yellow arrow) containing red blood cells in SCAPsiCdc42-Exo and SCAPML141-Exo group compared to the SCAPvehicle-Exo group. Scale bar = 50 μm. i Western blot and Pull-down assay showed that SCAP-Exo had higher levels of Cdc42 expression than that in SCAP, while the Cdc42-GTP expression was weaker in SCAP-Exo. j Immunofluorescence staining showed that Cdc42-EGFP-labeled proteins derived from SCAP-Exo (green) were expressed steadily in the cytoplasm of HUVECs in the primary culture, as well as in the 3rd and 6th passages. Scale bar = 100 μm. k Laser confocal microscope image showed the co-localization of SCAP-Exo-derived Cdc42-mCherry (red) and Cdc42 (green) in the cytoplasm of HUVECs. Slides were counterstained with DAPI (blue). Scale bar = 50 μm. n = 5 in each group. **P < 0.01, ***P < 0.001; Error bars: mean ± SD.

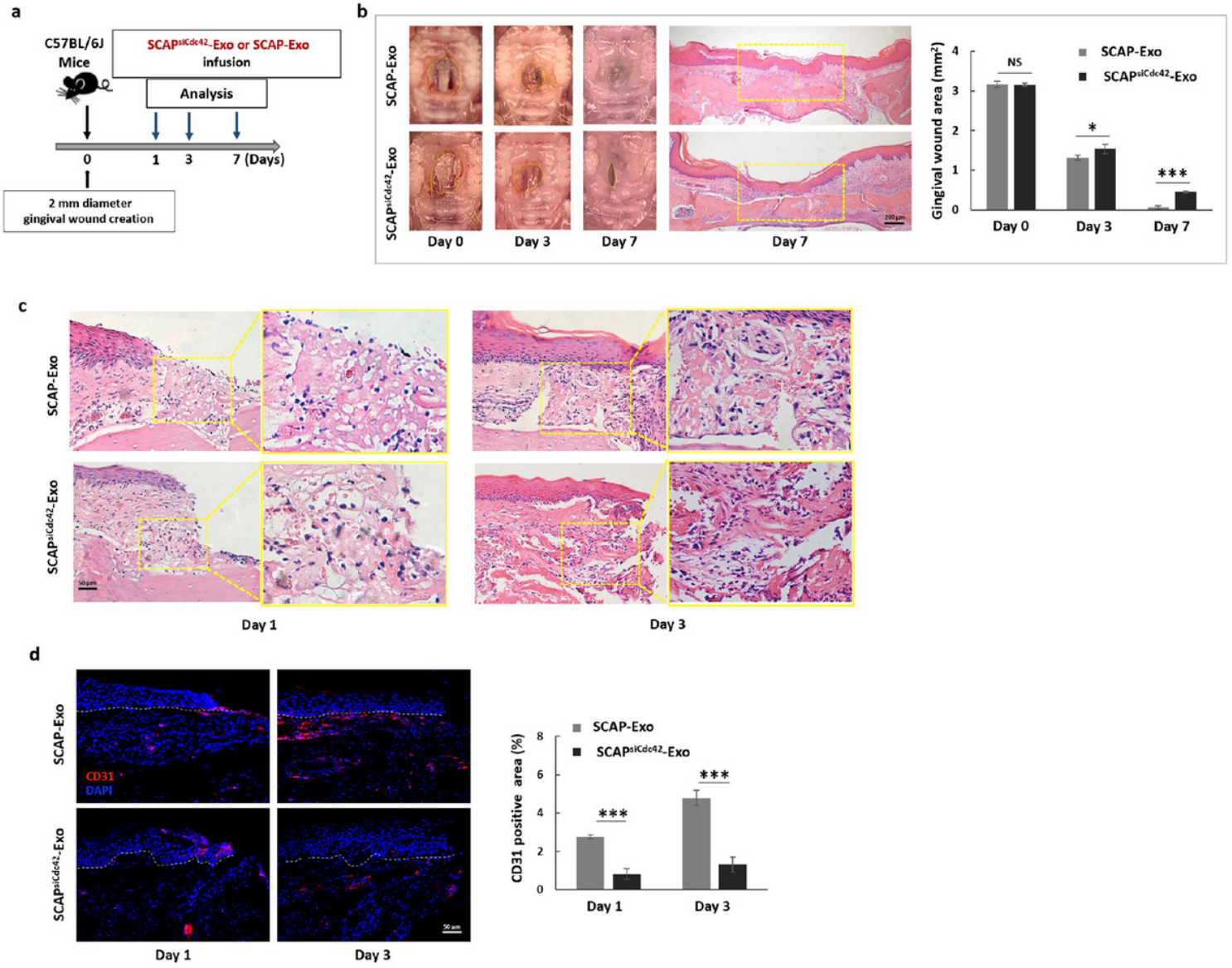

Figure 5

SCAP-Exo facilitated wound healing in the palatal gingiva via Cdc42. a Schema indicating the experimental design for SCAP-Exo or SCAPsiCdc42-Exo infusion in the gingival wound in palate of mice. b Representative images and quantification of gingival wound area in SCAP-Exo and SCAPsiCdc42-Exo group. The wound healing of palatal gingiva was significantly delayed in SCAPsiCdc42-Exo group at 3, 7 days post-wounding compared to SCAP-Exo group. H&E staining showed that the thickness of connective tissue (yellow segment) in SCAPsiCdc42-Exo group was thinner than that in SCAP-Exo group at 7 days post-wounding. Scale bar = 200 μm. c The histological views showed less newly formed blood vessels containing red blood cells in the gingiva wound of SCAPsiCdc42-Exo group at 1, 3 days post-wounding when compared with SCAP-Exo group. Scale bar = 50 μm. d Immunofluorescence staining and quantification showed that the percentage of CD31 positive area (red) in SCAPsiCdc42-Exo group was lower than that in SCAP-Exo group at 1, 3 days post-wounding. The epidermis and connective tissue were separated by the white dotted line in the images. Slides were counterstained with DAPI (blue). Scale bar = 50 μm. n = 5 in each group. NS: $P > 0.05$, *$P < 0.05$, ***$P < 0.001$; Error bars: mean ± SD.

Supplementary Files

This is a list of supplementary files associated with this preprint. Click to download.

- Supplementaryinformation.docx
- AdditionalFile1.pdf
- AdditionalFile2.pdf
- AdditionalFile3.pdf
- AdditionalFile4.pdf
- AdditionalFile5.pdf
- AdditionalFile6.pdf